Exfoliated Flexible Photonic Crystal Slabs for Refractive Index and Biomolecular Sensing

Fabio A. Kraft, Jan Schardt, Deborah Kitzler, Andreas Latz, and Martina Gerken, *Senior Member, IEEE*

***Abstract*— Using the optical transduction properties of 1-D photonic crystal slabs (PCSs) is a promising approach for label-free biosensing in the field of flexible and wearable biosensing. In this work, we demonstrate the fabrication of flexible PCSs (f-PCSs) via an exfoliation method from rigid PCSs. We investigate the processing effect on the optical properties and show that the optical resonances are maintained, but affected. The quality factor changes from 50 to 31 for the transverse electric (TE) mode and from 187 to 136 for the transverse magnetic (TM) mode after the process. We demonstrate the use of f-PCS for refractive index sensing and achieve a limit of detection (LOD) of $3.6E^{-4}$ refractive index units (RIUs). Furthermore, we introduce vapor-phase functionalization of the f-PCS and show the first results of biosensing of antibodies from diluted feline serum.**

***Index Terms*— 1-D photonic crystals, biosensing, flexible structure, microfluidics, refractive index sensing.**

I. Introduction

WEARABLE sensors are highly promising for continuous monitoring of one's health status [1]. The last years have shown that flexible electronics can be used to monitor the physical and chemical parameters from sweat [2], [3]. In order to minimize the invasiveness of the wearable sensors, great effort is being focused on wireless transmission to omit connecting wires [4]. Another possibility of noncontact and label-free readout is on the basis of optical transducers, among which 1-D photonic crystal slabs (PCSs) have been established as a technology platform [5], [6].

In our case, PCSs are 1-D nanostructured waveguides of 30, 45, or 60 nm depth with a period length of 370 nm. The waveguide is formed by a layer with a high refractive index such as titanium dioxide (TiO_2) or niobium pentoxide (Nb_2O_5) [7], [8]. Upon illumination, the nanostructure couples part of the light resonantly into the waveguide leading to a propagation of light within the waveguide. The propagating light is called a guided mode resonance (GMR) and dips in the transmission spectrum occur due to the destructive interference of the resonance with the incident light. The electrical field distribution of the GMR extends out of the waveguide layer and is sensitive to refractive index changes in the superstrate [9]. Changes of the superstrate refractive index lead to a shift of the resonance position. These changes can be read out via a spectrometer, an intensity-based or an interferometric approach [10], [11], [12]. All of these detection methods are based on rigid PCSs and are hence not suitable for a flexible application. First, endeavors into flexible PCSs (f-PCSs) have been carried out by Privorotskaya et al. [13] as well as Karrock et al. [14]. Both of them have used the effect that stretching the PCS leads to a change in resonance position, as they are based on stretchable high refractive index layers. However, for a flexible biosensing application, it is detrimental if the optical properties change upon mechanical strain, as the mechanical and biosensing signals would interfere. In this work, we introduce a novel approach for fabrication of f-PCS based on exfoliation of rigid PCS. In Fig. 1(a) and (b), an example and a rendering of an exfoliated f-PCS are depicted. We show that the optical properties of the exfoliated f-PCS are preserved, alas affected after the process. Yet, they retain their refractive index as well as biosensing capabilities. Furthermore, we demonstrate the combination of the f-PCS with a microfluidic for integrated sensing, as shown in Fig. 1(c) and (d).

In Section II, we describe the different materials and methods needed. Section III shows the experimental

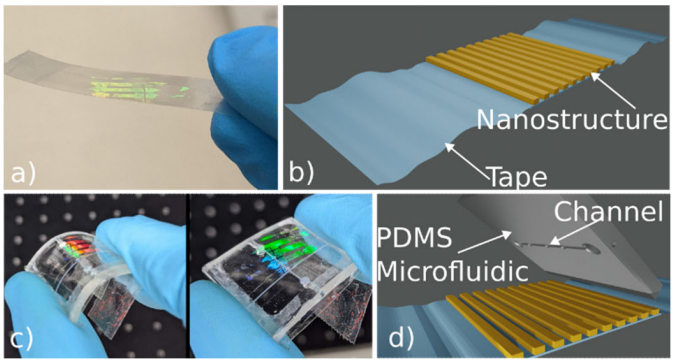

Fig. 1. (a) Image of the f-PCS on adhesive tape after the exfoliation process. (b) Visualization of the f-PCS. (c) f-PCS combined with a microfluidic under bent and relaxed conditions. (d) Visualization of (c), where the f-PCS and the PDMS microfluidic are separated.

Manuscript received 5 December 2022; accepted 31 December 2022. Date of publication 5 January 2023; date of current version 7 July 2023. This work was supported by the Federal Ministry for Economic Affairs and Climate Action (BMWK) on the basis of a decision by the German Bundestag under Grant ZF4558806SB9. An earlier version of this paper was presented at the 2022 IEEE International Conference on Flexible and Printable Sensors and Systems (FLEPS) [DOI: 10.1109/FLEPS53764.2022.9781592]. *(Corresponding author: Fabio A. Kraft.)*

Fabio A. Kraft, Jan Schardt, and Martina Gerken are with the Chair for Integrated Systems and Photonics, Department of Electrical and Information Engineering and the Kiel Nano, Surface and Interface Science KiNSIS, Kiel University, 24143 Kiel, Germany (e-mail: fkr@tf.uni-kiel.de).

Deborah Kitzler is with the Georgia Institute of Technology, Atlanta, GA 30332 USA.

Andreas Latz is with the Veterinary Diagnostics Department, NovaTec Immundiagnostica GmbH, 63128 Dietzenbach, Germany.

Digital Object Identifier 10.1109/JFLEX.2023.3234894

characterization of the f-PCS with regard to their microscopic as well as nanoscopic structure and their ability of sensing refractive index changes, detecting the binding of antibodies from diluted feline serum. The obtained results are discussed as they are being described. The conclusion is drawn in Section IV.

II. Materials and Method

A. Mathematical Background

PCSs show a dip in transmission when illuminated. GMRs are observed as peaks in the transmission spectrum of a PCS when they are illuminated between two orthogonally crossed polarizers [15]. The mathematical description is derived from [16]. For near normal incidence onto the surface of the PCS, the governing equation of the first-order GMR is given by

$$\lambda_{\mathrm{GMR}} = n_{\mathrm{eff}}\Lambda \tag{1}$$

known as the Bragg equation. Here, λ_{GMR} is the wavelength position of the GMR, n_{eff} is the effective refractive index of the quasi-guided mode, and Λ is the period length of the nanostructure. When the illumination is out of the normal plane, (1) has an angular dependency, which is described by [17]

$$\lambda_{\mathrm{GMR}} = n_{\mathrm{eff}}(\Lambda \pm \sin\Theta). \tag{2}$$

The angle Θ describes the angle of incidence with respect to the normal vector of the surface. It is to be noted that due to the plus–minus sign, two mode branches shifting into the blue and red spectrum occur under out-of-plane illumination.

In order to estimate the functionality of the f-PCS, we calculate the limit of detection (LOD) when exposed to different concentrations of water–ethanol mixtures. The combination of water and ethanol allows for tuning of specific refractive indices and is used as a proxy for biosensing abilities. These changes are called bulk refractive index changes [18]. The corresponding LOD is calculated as follows:

$$\mathrm{LOD} = 3\sigma/S. \tag{3}$$

In the above equation, the noise is denoted by σ and the sensitivity is expressed by S. The sensitivity S is described by

$$S = \Delta\lambda_{\mathrm{GMR}}/\Delta n \tag{4}$$

where Δn is the induced difference of the refractive index and $\Delta\lambda_{\mathrm{GMR}}$ is the observed resonance shift.

For evaluation of the optical properties, the quality factor (Q-factor) is used. It is described by

$$Q = \lambda_{\mathrm{GMR}}/\mathrm{FWHM}. \tag{5}$$

where FWHM stands for the full-width at half-maximum of the resonance peak.

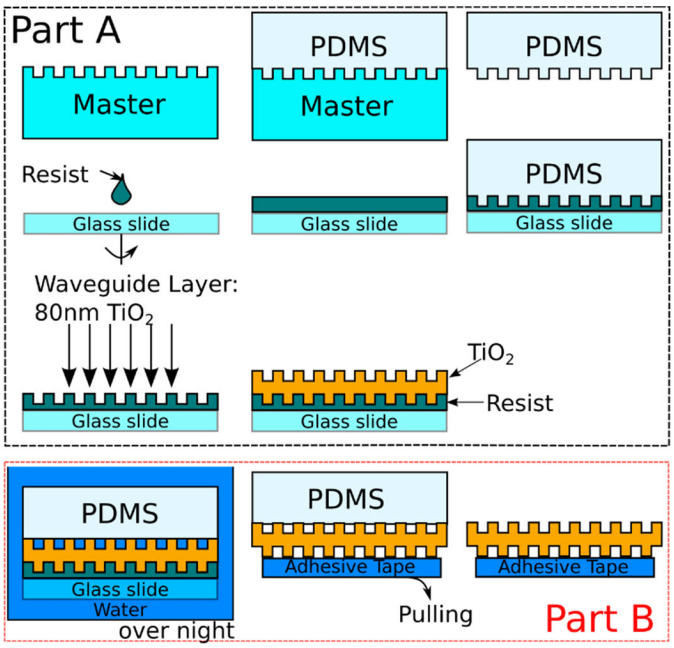

Fig. 2. Process flow for creating (a) PCS and (b) subsequent creation of f-PCS.

B. PCS Fabrication

The PCS is created via nanoimprint lithography [19]. A negative mold of poly(dimethylsiloxane) (PDMS) (Dow, Sylgard 184 and curing agent at a ratio of 8:1) is created from a nanostructured master. The stamp is then imprinted into a spincoated film of UV nanoimprint resist (AMONIL,[1] AMO GmbH) on a glass substrate of size 25 × 25 mm^2. The stack is UV cured for 1 min and the PDMS is peeled off, exposing the nanostructured resist. We want to stress that the primer (AMOPRIME,[1] AMO GmbH) is omitted, which facilitates the exfoliation method. Afterward, an 80-nm layer of high index material, in this case TiO_2 (Kurt J. Lesker, EJUTIO2403TK4), is sputtered onto the nanostructured substrate. The fabrication is schematically shown in Fig. 2(a).

C. Flexible Photonic Crystal Slabs (f-PCSs)

In order to fabricate f-PCSs, the PCS and a flat PDMS membrane of 2 mm in thickness are stuck together and placed in water for overnight incubation. They remain bound due to the adhesive properties of PDMS. The water reduces the adhesive properties of the resist AMONIL[1] such that the PCS remains on the PDMS membrane when pulled off. By applying the adhesive tape, the PCS is transferred to it. This is shown in Fig. 2(b). The flexible nature of the f-PCS is visible in the photographs in Fig. 1(c). In this case, the adhesive tape from tesafilm[1] eco & clear BNR 57035 (Tesa SE, Norderstedt, Germany) is used. An analysis of the optical influence of different adhesive tape substrates is given in the Appendix.

D. PDMS Microfluidic

The microfluidics are created via a combination of lithographic and molding processes [20]. A silicon wafer is used

[1]Registered trademark.

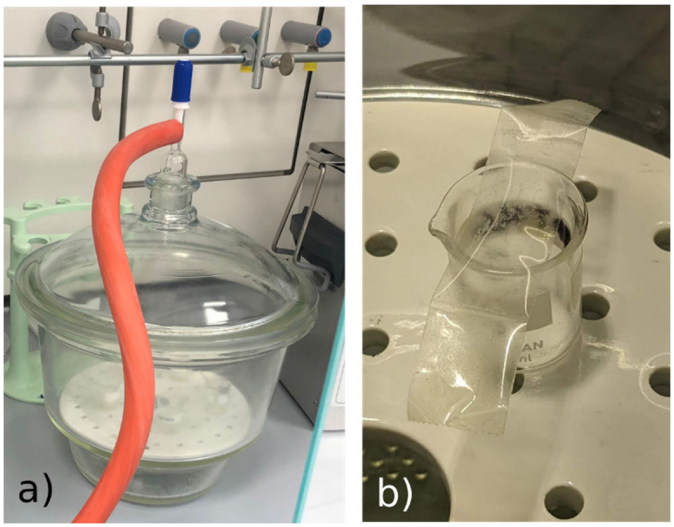

Fig. 3. (a) Desiccator is connected via the orange tube to the house vacuum line. It contains the beakers with the silanization or crosslinking solution for functionalization. (b) Photograph of adhesive tape placed upside down onto the beaker such that the active surface is exposed to the evaporating liquid.

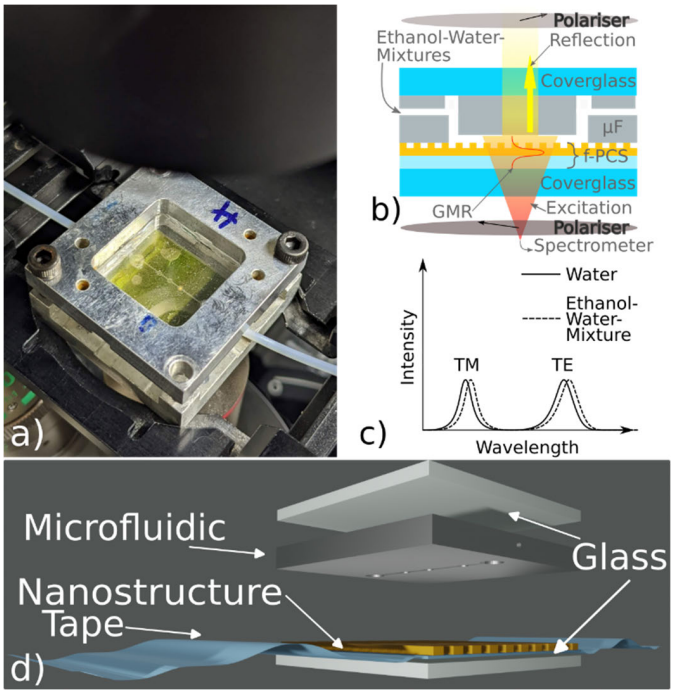

Fig. 4. (a) Setup for the integrated microfluidic sensing is shown. The inlet and outlet tubes are visible. (b) Schematic to the measurement setup (a), μF stands for microfluidic. (c) Schematic of the resonance shift induced by changes of the bulk refractive index. (d) Visualization of the stack in (a).

as a process basis and the negative photoresist SU-8 (Micro Resist Technology, SU8-50) is spincoated onto the wafer at 1000 r/min for 1 min. A mask containing the microfluidic layout is transferred into the resist via photolithography. After development, the projected structure is visible on the silicon wafer. Then, PDMS is cast onto the wafer and degassed to eliminate air bubbles. Afterward, the wafer is placed in an oven at 130 °C for 30 min. After cooling, the PDMS is peeled off and the microfluidic form is seen in the PDMS. The microfluidic forms are cut out into areas of 25 × 25 mm^2. For the experiments here, we apply additional holes for tubing via biopsy punches. The resulting microfluidic channel is 100 μm in depth and consists of three chambers of 1.5 mm radius, which are connected via 200-μm-wide channels.

E. Functionalization and Immobilization

We carry out surface functionalization analogously to previously published processes [6]. However, in order to avoid direct contact of organic liquids with the adhesive tape, the functionalization takes place in a vapor phase [21]. First, we place the f-PCS in a plasma reactive ion etching chamber (Sentec, SI100) for 3.5 min with 100-W power with an oxygen flow of 8 sccm to induce an activated surface. Afterward, a 400-μL silanization solution consisting of 260 μL of (3-aminopropyl)triethoxysilane (APTES) (440140, Sigma-Aldrich) dissolved in 24.5 mL of dry methanol (322415, Sigma-Aldrich) is placed in a beaker onto which the surface activated f-PCS is placed. The active surface of the f-PCS faces down toward the liquid. The beaker and the f-PCS are then placed into a desiccator, which is connected to a vacuum pump. Fig. 3 shows these steps. The vacuum facilitates the evaporation of the solutions. The f-PCS is being left exposed for 1 h. After the silanization process, we place the f-PCS on a heat plate at 110 °C for 20 min. The subsequent steps use a crosslinking solution, which consists of 200-mg 1,4-phenylendiisothiocyanat (PDITC) (258555, Sigma-Aldrich) dissolved in 1 mL of pyridine (270970, Sigma-Aldrich) and 9 mL of N,N-dimethylformamid (DMF) (227056, Sigma-Aldrich). The f-PCS is placed again with its active face down onto a beaker, into which 400 μL of the crosslinking solution is placed. The beaker is placed once more in a desiccator and is evacuated. We expose the f-PCS for 3 h. Afterward, the f-PCS is left in a fume hood for 20 min for desorption of excess crosslinking molecules on the surface.

For the immobilization, the surface functionalized f-PCS is placed in a wet chamber and two 1-μL droplets of a 100-μg/mL recombinant protein A/G (ThermoFisher Scientific, 21186) diluted in Dubelccos' phosphate-buffered saline (DPBS) (D8537, Sigma-Aldrich) are placed onto the crosslinked f-PCS surface by hand and left for overnight incubation. Next, the remaining f-PCS surface is passivated by adding the 1-mg/mL bovine serum albumin (BSA) solution and letting it sit for 1 h. The BSA solution is created by diluting 1 mg of BSA (A2153, Sigma-Aldrich) in 1 mL of DPBS. Finally, the excess BSA is washed off with DPBS and deionized water and the f-PCS is dried with nitrogen.

F. Measurement Setups

1) Integrated Microfluidic Setup: The f-PCS is used in two modes for the characterization measurements. The first mode is shown in Fig. 4(a) and (d). In this case, we place the f-PCS between glass plates for easier analysis. The glass plates are omitted in a wearable application. The f-PCS is placed on top of a glass plate and a PDMS microfluidic with a channel depth of 100 μm is placed on top. The other side of the

PDMS microfluidic is sealed off with an additional glass plate. This stack is mounted into a metal frame and placed into a microscope and illuminated with a broadband light source. The stack is placed between two orthogonally crossed polarizers in order to suppress any excitation light [15]. The emitted light from the surface of the f-PCS is gathered via an objective and led to a spectrometer (Andor, Shamrock 500i). A spectrum was recorded every second. Via an external microfluidic pump (Fluigent MFCS-EZ), water–ethanol mixtures with a weight percentage of 5, 10, 15, and 20 were pumped through the microfluidic channel to induce bulk refractive index changes. The refractive indices of the mixtures are measured with an Abbe-refractometer (Bellingham and Stanley Ltd., Model 60/ED) beforehand. The changes are expressed in refractive index units (RIUs) and the shifts of the guided mode position are tracked via Lorentzian peak fitting of the transverse magnetic (TM) mode. The qualitative effect of resonance shifting is sketched in Fig. 4(c).

2) Biosensing Setup: The second mode is analogous to the integrated microfluidic setup. Similar to the above, the f-PCS was placed on top of a glass slide for ease of use. As stated above, the glass plates are omitted in a wearable application. Above the f-PCS, a circular gasket is placed, which creates a cavity into which liquids are injected from butterfly cannulas. Two butterfly cannulas are used for in-and-outflow [22]. The gasket is sealed off with a second glass substrate and mounted again on the microscope. This reservoir is referred to as the fluid chamber and is shown in Fig. 5(a) and as a visualization in Fig. 5(d). For biosensing demonstration, feline serum (Equitech-Bio, Inc., FS05-0100, Lot: 180514-0105) is diluted in DPBS with a factor of 1–500 and injected via the butterfly cannulas. The analysis of cat serum assesses the ability of f-PCS to detect immunoglobulin G (IgG) from samples of biological origin. For this, the f-PCS is functionalized with 1 μL of 100-μg/mL recombinant protein A/G diluted in DPBS, which binds IgG with a high affinity. Other subclasses, such as immunoglobulin M (IgM) and immunoglobulin A (IgA), show a weak affinity. The immobilized mass of protein A/G is approximately 100 ng. The immobilization concentration is at similar levels as other published label-free measurement setups [23], [24]. Cat serum antibodies of type IgG range between 19 and 28 mg/mL [25], [26]. A dilution of 500 leads to an approximate level of added IgG in the range of 38–56 μg/mL.

In Fig. 5(b), the thin blue and orange lines indicate areas, where spectra for binding to immobilized protein A/G spots are recorded and the green lines indicate positions for the reference spectra. The bold circles were first intended for referencing, but their limited free area within the circle rendered it unfeasible. The position is stepped through with a stepping motor and the wavelength shifts were evaluated by cross-correlating the acquired spectra. Fig. 5(c) shows an image of droplets for immobilization incubation.

3) Goniophotometer Setup: In order to analyze the angular optical properties of the PCS and f-PCS, a goniophotometer setup is used [27]. This setup allows for precise angular rotation of the PCS and f-PCS while recording their spectrum. It is illuminated with a white light source and the transverse

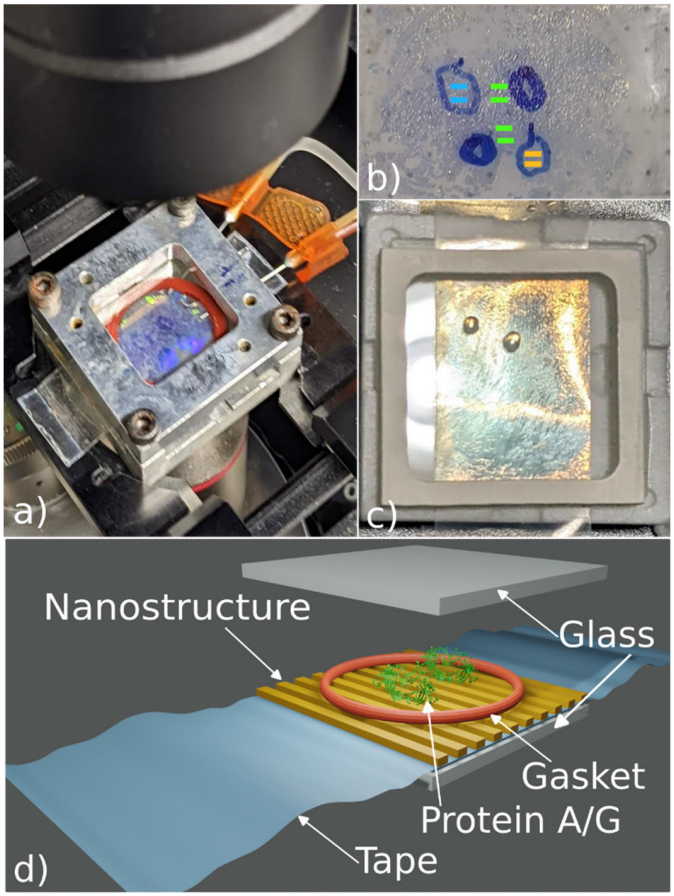

Fig. 5. (a) Setup for biosensing. The f-PCS is sealed off with a gasket (red) into which butterfly cannulas are injected. These function as inlet and outlet of the fluid chamber. The circles indicate the areas of immobilized protein A/G. (b) Photograph of spots and areas used for acquiring spectra of areas immobilized with protein A/G (blue and orange) and reference areas (green). (c) Image of spots placed on an f-PCS for incubation. (d) Visualization of the setup in (a).

electric (TE) and TM modes are excited separately by using a linear polarizer in front of the slabs. The shifts of the resonance as predicted by (2) are recorded. The f-PCS is combined with a glass slide to have a flat surface. For evaluation, each angle-dependent spectrum is set into the relation of the unperturbed light-emitting diode (LED) spectrum recorded at 0°.

III. Results and Discussion

A. Optical and Mechanical Properties

The resonance behavior is affected by several factors, including the optical properties of the adhesive tape, the exfoliation process, and the history of deformation. The properties of two different tape types are discussed in the Appendix. Figs. 6 and 7 show that the overall resonance position is not affected. The observed shift can be attributed to inhomogeneities of the high refractive index layer thickness [12]. However, the Q-factors are affected, as shown in Figs. 6 and 7. In Fig. 7(a), the TM mode for the f-PCS is skewed. In addition, both modes are wider, leading to a decrease of the Q-factor. The dip in the transmissions of the TE mode in Fig. 7(a) may be related to the phase offset of different photonic crystal cells leading to a changed coherence

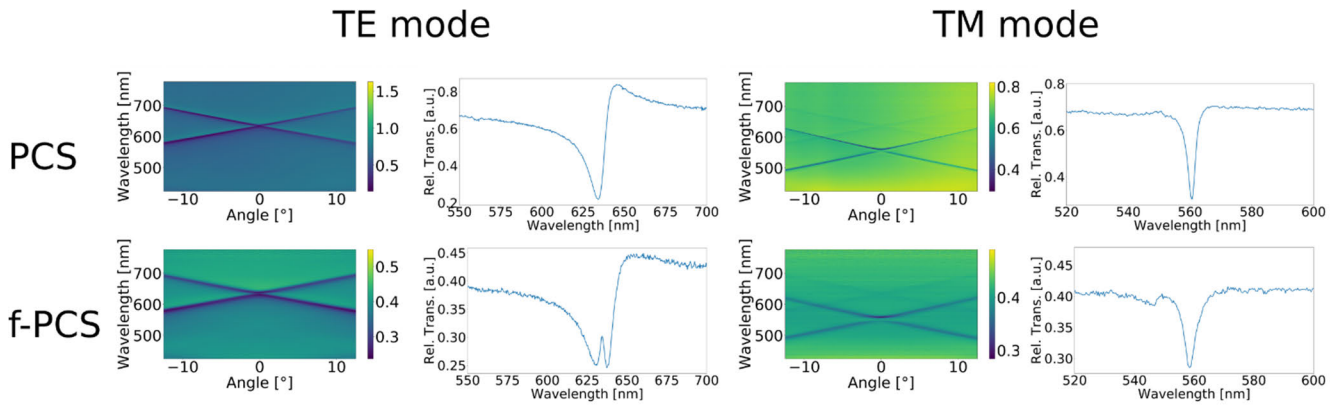

Fig. 6. Angle-dependent spectral behavior of the TE and TM GMR for the rigid (PCS) and f-PCS as described by (2). For each plot, the 0° spectrum is shown to illustrate the quality of the resonance. The y-axis describes the relative transmission in arbitrary units.

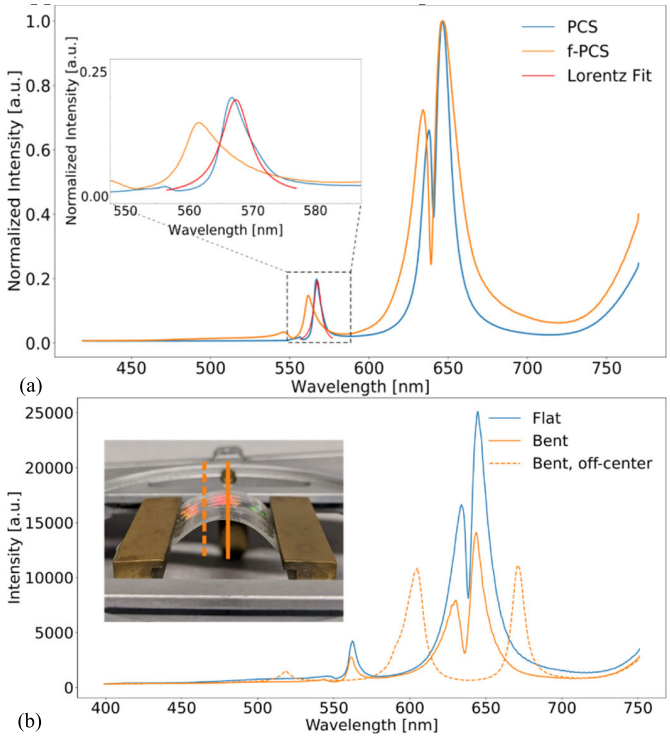

Fig. 7. Resonance behavior of a rigid and f-PCS. (a) Normalized resonance spectrum of rigid and f-PCS. The blue line shows the spectrum for the rigid PCS, whereas the orange line shows the spectral behavior for f-PCS. The inlet zooms into the TM mode of the resonance and depicts a Lorentzian fitting. (b) Resonance behavior of an f-PCS under flat and bent conditions. The resonance behavior for the bent condition is evaluated at two points indicated by a solid dashed line.

behavior [28]. The resulting Q-factors are 50 and 187 for the TE and TM modes on PCS and 31 and 136 for the TE and TM modes on the f-PCS, respectively. These values are derived from the goniophotometer data shown in Fig. 6. In addition, Fig. 7(b) shows the influence of bending on the achievable Q-factors. For a flat f-PCS, the obtained Q-factor is 137. When the f-PCS is measured at the vertex of a bent f-PCS, the Q-factor is slightly reduced to 126. Fig. 7(b) shows the splitting of the modes measured off-center under bent conditions analogous to the behavior shown in Fig. 6. In the past, resonant optical structures with very different Q factors have been used successfully for biosensing. For example, plasmonic resonator shows a Q-factor around ten, while microsphere resonators may have a high Q-factor of 10^8–10^9 [29], [30]. Conteduca et al. [31] argued that for label-free sensing, an interplay of amplitude and Q-factor is the limiting factor. We target intermediate Q factors of around 100–200 to achieve a good amplitude signal. The spectra of Fig. 7(b) were taken with the same settings. Comparing the Q-factor and amplitude of the TM modes and assuming no change in sensitivity and noise, the influence of bending on the LOD for the bent f-PCS is modeled to be reduced by a factor of approximately 0.4. This leads to a theoretical LOD of $6E^{-4}$ RIU, which is sufficient for refractive index and biomolecular sensing [6]. These theoretical findings need to be corroborated with experimental tests in future analyses.

Furthermore, both modes exhibit a decrease of their respective suppression level for the f-PCS. This can be attributed to the cell formation within the f-PCS, which is discussed in more detail in the following. Due to the fractured structure, more light passes through these cracks of f-PCS, which in turn cannot be used for the resonance effect and reduces coupling efficiency. In addition, the boundaries of the cells are scattering centers contributing to the decreased efficacy of the resonance effect. The single cells act as individual PCS of reduced size. Boye et al. [32] argued that the Q-factor of the resonance is strongly affected by the size of the PCS. They have shown that a reduction in size leads to a decrease of the Q-factor for the same design parameters, which is an explanation of the reduced Q-factors observed in this work. The TE and TM modes of the f-PCS also show a separation of the peaks under 0° illumination, when compared to the PCS behavior. For continuous corrugated waveguides, it has been shown that for perpendicular illumination, only one mode is supported for propagation within the waveguide, which is observed for the PCS case [33]. Further investigations as to why two modes are supported in the f-PCS case need to be performed.

The flexibility of the f-PCS is enabled by the cracking of the high refractive index layer upon external stress. In the rigid PCS, the high refractive index layer is continuous. However, due to the applied mechanical stress during the exfoliation

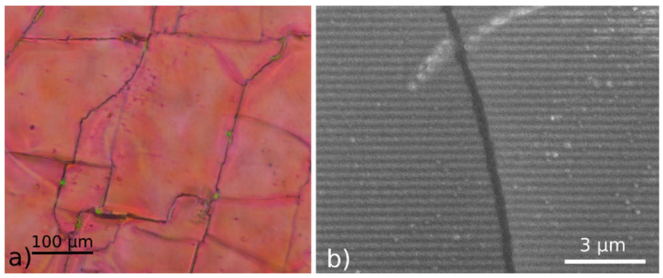

Fig. 8. (a) Image of the surface of the f-PCS illuminated between two orthogonally crossed polarizers. The fractures between the single cells, which gives the photonic crystal its flexibility, are visible. (b) SEM image of the f-PCS at the interface of two photonic crystal cells. The white parts are particles, which are stuck to the surface.

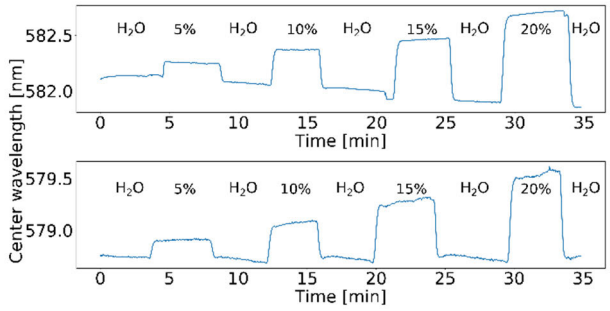

Fig. 9. Refractive index sensing properties of the PCS (top) and f-PCS (bottom) compared to one another. Water and water–ethanol exposure intervals are indicated. The center wavelength was tracked via Lorentzian fitting.

process, energy is released by cracking of the homogenous layer to singular cells. This behavior is shown in Fig. 8(a). The single PCS cells are disconnected as can be seen by the fractures on the surface. The fractures appear black as the excitation light is blocked due to the orthogonally crossed polarizers [15]. Their resonance effect is clearly visible, as they appear deep red. This is in concordance with the spectrum in Fig. 7. The cells of the PCSs are the basis for the flexibility, as they can now adjust to movement of the supporting material. Fig. 8(a) shows that the cell shape is not homogenous in size and shape but shows a size distribution, which is influenced by fabrication. The cells vary in lateral dimension between 10 and 500 μm. A scanning electron microscopy (SEM) image of a fractured PCS is shown in Fig. 8(b). The nanostructure of the f-PCS is clearly visible. It is divided by a crack and has its grating slightly offset vertically, indicating a movement of the PCS cells with respect to one another.

B. Refractive Index Sensing Properties

The sensing properties are evaluated by flowing water and ethanol–water mixtures with a mass concentration up to 20% in steps of 5% above both specimens. The recorded wavelength shift for the PCS and f-PCS is plotted in Fig. 9. The summarized data are given in Table I. The data show that a decrease of the Q-factor does not influence the overall sensitivity of the PCS and f-PCS. Both sensitivities are with 65 and 72 nm/RIU comparable. However, the average noise is with 0.018 nm for the f-PCS twice as high as for the PCS, which has a value of 0.009 nm. This results in a decreased LOD for the f-PCS.

TABLE I
MEASURED PERFORMANCE PARAMETERS FROM RIU CHANGES FOR f-PCSs AND RIGID PCSs

Type	Ethanol-water-mixture [wt%]	3σ - Noise [nm]	Diff. [nm]	Sensitivity [nm/RIU]	LOD [RIU x 10^{-4}]
PCS	5	0.005	0.12	61	0.84
	10	0.004	0.29	60	0.74
	15	0.009	0.55	70	1.3
	20	0.017	0.79	69	2.5
f-PCS	5	0.012	0.17	84	1.3
	10	0.02	0.34	69	2.9
	15	0.013	0.55	70	1.8
	20	0.024	0.78	68	3.6

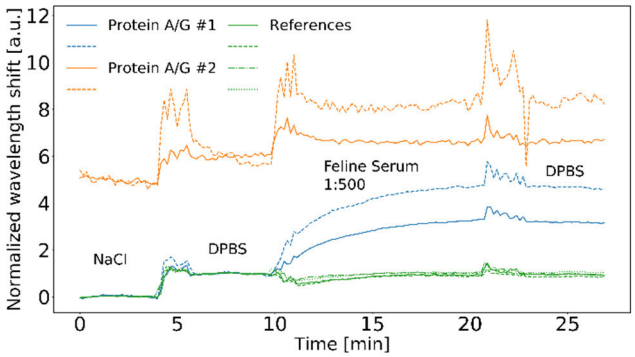

Fig. 10. Resonance shift behavior for differently functionalized surfaces on an f-PCS. The blue and orange plots show the behavior where protein A/G is immobilized, which binds any type of antibody. The orange lines are offset by a value of five for better visualization. The green data are reference spots. The wavelength shift is normalized to the induced refractive index change from 1.3330 to 1.3343 RIU. The added diluted feline serum corresponds to an injection of IgG in a range of 38–56 μg/mL.

The highest LOD is $2.5E^{-4}$ RIU for the PCS compared to $3.6E^{-4}$ RIU for the f-PCS. Further improvements are expected by custom tailoring of the fitting type [34]. Furthermore, the f-PCS is more stable toward the influence of the water–ethanol mixture, as is evident by the absence of drift, when exposed to water compared to the rigid PCS. The rigid PCS might be susceptible to water inclusion in the imprint resist below the waveguide, which is also used for the exfoliation effect. The slightly more prominent drift of the f-PCS when exposed to ethanol might stem from the fact that ethanol is a solvent and it dissolves the adhesive of the tape.

C. Biosensing Demonstration

The f-PCS is functionalized following the procedure described in Section II-E. The acquired data for the binding of antibodies to the surface of the f-PCS are shown in Fig. 10. Initially, the liquid chamber is filled with a solution of 1-mg/mL NaCl in water. Then, DPBS is injected into the fluid chamber. The recorded refractive indices (Krüss, DR-201-95) are 1.3330 and 1.3343 RIU. This corresponds to a change of $1.3E^{-3}$ RIU. This bulk refractive index change

is used to normalize the spots to their sensitivity. Following the buffer step, the diluted feline serum is injected. Serum is used, as it contains an excess of IgG antibodies, which binds to the immobilized protein A/G with a high affinity [35]. Furthermore, using serum in combination with protein A/G determines the ability of f-PCS to detect IgG antibodies from samples of biological origin. The immobilization of 1 μL of protein A/G with a concentration of 100 μg/mL is in a similar range as other published feasibility studies for label-free sensing systems [23], [24]. As mentioned above, antibodies of type IgG in cat serum are in the range of 19–28 mg/mL [25], [26]. A dilution of 500 leads to estimated added IgG levels in the range of 38–56 μg/mL. Cat serum is used as it was easily supplied by the collaborating company NovaTec Immundiagnostica GmbH (Dietzenbach, Germany).

The data in Fig. 10 show that the regions with the immobilized protein A/G show a different behavior than the reference region. The blue curves show a common kinetic of a binding curve [36]. At injection, the orange lines show a jump in their signal and remain at that level for the remainder of the experiment. An explanation might be rooted in the distribution of receptors on the surface. Urbanowska et al. [37] have shown that immobilization of proteins on surfaces shows inhomogeneous distribution, e.g., a droplet of capturing proteins forms a ring shape. Sampling via the slit of a spectrometer integrates along a line on the f-PCS [rf. Fig. 11(b)]. Assuming a ring-shaped immobilization, this might lead to an averaging of binding and other superimposed effects, giving rise to the observed behavior for the orange lines. The reference signals in green show a dip after the injection of the diluted serum and then reach again the level prior to injection, indicating no mass change on the surface.

The obtained data illustrate that f-PCS is able to detect IgG antibodies from real biological samples at relevant biological concentrations. The detection of 38–56 μg/mL of IgG is lower or in a similar range of published work by Xiao et al. [23] and Coskun et al. [35], who demonstrated the detection of IgG antibodies in concentrations of 10 and 200 μg/mL with immobilized protein A/G, respectively. Detecting IgG at these concentrations is promising for the analysis of specific IgG antibodies. For instance, influenza IgG antibodies are found in undiluted human serum at levels between 12.5 and 135 μg/mL [38]. Furthermore, the obtained signal changes due to binding indicate that lower concentrations of IgG antibodies are detectable. In a heuristic evaluation and assuming a linear behavior, the added IgG concentration might be lowered by a factor of 10 and still cause a signal change, which approximately corresponds to one-third of a normalized step size. The detectable levels are expected to be in the range of single-digit μg/mL concentrations. Furthermore, it is an option to omit here the used dilution in order to adapt to different concentration levels of analytes. However, surface-to-protein interaction is known to be sensitive. Influences, such as steric hindrance, choice of buffer, and antigen, have a strong influence on the sensitivity and specificity of the system. In order to address these shortcomings, titration experiments with different immobilization concentrations as well as serum dilutions need to be performed in the future.

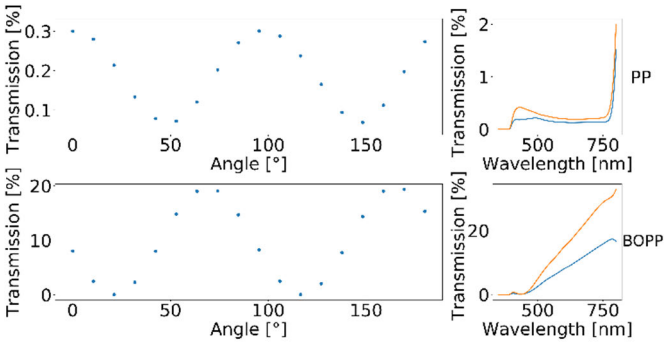

Fig. 11. Polarizability of the two different types of carrier tape examined under crossed polarizers. The first rows show the data for Tesa 57035 and PP is short for polypropylene. The second row shows the values for Tesa 57375, and BOPP means biaxially-oriented polypropylene. The first column shows the transmission percentage obtained at 600 nm for different rotation angles. The second column shows the spectra at the transmission minimum (blue) and maximum (orange) for each carrier material.

IV. Conclusion

In this article, we have shown a novel approach of fabricating f-PCSs from a rigid predecessor by using an exfoliation method based on commercially available adhesive tape. We elucidated that the flexibility stems from the fracturing of the waveguiding layer giving rise to a structure of multiple photonic crystal cells. We have demonstrated that the f-PCS retains their refractive index sensing ability, yet they show a decrease in their Q-factor and an increase in their noise, which leads to a decreased LOD compared to the rigid PCS. We introduced a method to functionalize f-PCS using a vapor-phase process. We demonstrated successful biosensing of IgG antibodies from diluted feline serum with the f-PCS and were able to detect IgG at levels of biological relevance. The detected levels of IgG are competitive to previously published work analyzing label-free sensing setups [23], [35]. The here shown work opens up the possibility for applications in wearable patches for health monitoring. To our knowledge, no previous work has shown biosensing on flexible photonic crystal slabs.

Appendix

When using adhesive tape based on polymers, one has to account for the polarizing abilities of the polymers. Here, we investigate the effect of two commercially available adhesive tapes from the company Tesa, with their article number 57035 and 57375. The substrate 57035 is made of polypropylene (PP) and 57375 is processed with biaxially oriented polypropylene (BOPP).

The polymer carrier material is analyzed by placing different polymers between two orthogonally crossed polarizers and measuring their respective transmission via a spectrometer (Carry 5000, Agilent) at rotation angle intervals of 10° for a half-rotation. The transmission value is evaluated at 600 nm.

The first column of Fig. 11 shows both carrier materials have a periodic polarization effect when measured between crossed polarizers. However, the adhesive tape made out of PP changes by 0.2% in its transmission, indicating a minor influence on the polarization state. The material consisting

of BOPP has a peak-to-valley value of 19%, demonstrating a significant influence on the polarization state. Furthermore, the spectral response of both materials is shown in the second column of Fig. 11. The substrate 57035 shows almost no effect on the polarization state over the entire visible spectrum. The BOPP, however, has an increasing dispersive property over the visual spectrum. The periodic effect of both substrates might be attributed to a crystalline structure of polymers induced during manufacturing. It has been reported that thin films of PP and BOPP exhibit birefringence and that the degree of birefringence is affected by the creation process. In turn, birefringence affects the polarization of light and can be used as an explanation for this behavior [39], [40]. Since both materials are of commercial origin, further analysis as to the exact underlying effect is limited.

REFERENCES

[1] W. Gao, H. Ota, D. Kiriya, K. Takei, and A. Javey, "Flexible electronics toward wearable sensing," *Acc. Chem. Res.*, vol. 52, no. 3, pp. 523–533, Mar. 2019, doi: 10.1021/acs.accounts.8b00500.

[2] M. Chung, G. Fortunato, and N. Radacsi, "Wearable flexible sweat sensors for healthcare monitoring: A review," *J. Roy. Soc. Interface*, vol. 16, no. 159, Oct. 2019, Art. no. 20190217, doi: 10.1098/rsif.2019.0217.

[3] S. M. Mugo and J. Alberkant, "Flexible molecularly imprinted electrochemical sensor for cortisol monitoring in sweat," *Anal. Bioanal. Chem.*, vol. 412, no. 8, pp. 1825–1833, Mar. 2020, doi: 10.1007/s00216-020-02430-0.

[4] W. Gao et al., "Fully integrated wearable sensor arrays for multiplexed in situ perspiration analysis," *Nature*, vol. 529, no. 7587, pp. 509–514, 2016, doi: 10.1038/nature16521.

[5] G. Zanchetta, R. Lanfranco, F. Giavazzi, T. Bellini, and M. Buscaglia, "Emerging applications of label-free optical biosensors," *Nanophotonics*, vol. 6, pp. 627–645, Jan. 2017, doi: 10.1515/nanoph-2016-0158.

[6] S. Jahns et al., "Handheld imaging photonic crystal biosensor for multiplexed, label-free protein detection," *Biomed. Opt. Exp.*, vol. 6, no. 10, pp. 3724–3736, 2015, doi: 10.1364/boe.6.003724.

[7] G. Pitruzzello and T. F. Krauss, "Photonic crystal resonances for sensing and imaging," *J. Opt.*, vol. 20, no. 7, Jul. 2018, Art. no. 073004, doi: 10.1088/2040-8986/aac75b.

[8] Y. Nazirizadeh, U. Lemmer, and M. Gerken, "Experimental quality factor determination of guided-mode resonances in photonic crystal slabs," *Appl. Phys. Lett.*, vol. 93, no. 26, pp. 10–13, 2008, doi: 10.1063/1.3058682.

[9] B. Kovacs, F. A. Kraft, Z. Szabo, Y. Nazirizadeh, M. Gerken, and R. Horvath, "Near cut-off wavelength operation of resonant waveguide grating biosensors," *Sci. Rep.*, vol. 11, no. 1, pp. 1–14, Jun. 2021, doi: 10.1038/s41598-021-92327-4.

[10] A. Kenaan, K. Li, I. Barth, S. Johnson, J. Song, and T. F. Krauss, "Guided mode resonance sensor for the parallel detection of multiple protein biomarkers in human urine with high sensitivity," *Biosensors Bioelectron.*, vol. 153, Apr. 2020, Art. no. 112047, doi: 10.1016/j.bios.2020.112047.

[11] B. T. Cunningham, "Photonic crystal surfaces as a general purpose platform for label-free and fluorescent assays," *JALA, J. Assoc. Lab. Autom.*, vol. 15, no. 2, pp. 120–135, Apr. 2010, doi: 10.1016/j.jala.2009.10.009.

[12] FF. A. Kraft, J. Blaesi, and M. Gerken, "Regions of interest and their influence on the limit of detection in an intensity-based refractive-index sensing setup," in *Proc. Biophotonics Congr.*, 2021, p. DM1A.3.

[13] N. L. Privorotskaya, C. J. Choi, B. T. Cunningham, and W. P. King, "Sensing micrometer-scale deformations via stretching of a photonic crystal," *Sens. Actuators A, Phys.*, vol. 161, nos. 1–2, pp. 66–71, Jun. 2010, doi: 10.1016/j.sna.2010.05.024.

[14] T. Karrock, M. Paulsen, and M. Gerken, "Flexible photonic crystal membranes with nanoparticle high refractive index layers," *Beilstein J. Nanotechnol.*, vol. 8, pp. 203–209, Jan. 2017, doi: 10.3762/bjnano.8.22.

[15] H. Luder, M. Paulsen, and M. Gerken, "Photonic crystal slab between orthogonal polarizers: Details on the guided mode resonance wavelength," *Opt. Quantum Electron.*, vol. 52, no. 3, pp. 1–14, Mar. 2020, doi: 10.1007/s11082-020-02296-7.

[16] M. Paulsen, L. T. Neustock, S. Jahns, J. Adam, and M. Gerken, "Simulation methods for multiperiodic and aperiodic nanostructured dielectric waveguides," *Opt. Quantum Electron.*, vol. 49, no. 3, pp. 1–14, Mar. 2017, doi: 10.1007/s11082-017-0918-6.

[17] M. Paulsen, S. Jahns, and M. Gerken, "Intensity-based readout of resonant-waveguide grating biosensors: Systems and nanostructures," *Photon. Nanostruct.-Fundam. Appl.*, vol. 26, pp. 69–79, Sep. 2017, doi: 10.1016/j.photonics.2017.07.003.

[18] Y. Nazirizadeh et al., "Sensitivity optimization of injection-molded photonic crystal slabs for biosensing applications," *Opt. Mater. Exp.*, vol. 3, no. 5, p. 556, 2013, doi: 10.1364/ome.3.000556.

[19] J. Buhl, D. Yoo, M. Köpke, and M. Gerken, "Two-dimensional nanograting fabrication by multistep nanoimprint lithography and ion beam etching," *Nanomanufacturing*, vol. 1, no. 1, pp. 39–48, May 2021, doi: 10.3390/nanomanufacturing1010004.

[20] E.-C. Yeh, C.-C. Fu, L. Hu, R. Thakur, J. Feng, and L. P. Lee, "Self-powered integrated microfluidic point-of-care low-cost enabling (SIMPLE) chip," *Sci. Adv.*, vol. 3, no. 3, pp. 1–12, Mar. 2017, doi: 10.1126/sciadv.1501645.

[21] S. Fiorilli et al., "Vapor-phase self-assembled monolayers of aminosilane on plasma-activated silicon substrates," *J. Colloid Interface Sci.*, vol. 321, no. 1, pp. 235–241, 2008, doi: 10.1016/j.jcis.2007.12.041.

[22] J. Blasi and M. Gerken, "Multiplex optical biosensors based on multi-pinhole interferometry," *Biomed. Opt. Exp.*, vol. 12, no. 7, pp. 4265–4275, 2021, doi: 10.1364/boe.426991.

[23] B. Xiao, S. K. Pradhan, K. C. Santiago, G. N. Rutherford, and A. K. Pradhan, "Topographically engineered large scale nanostructures for plasmonic biosensing," *Sci. Rep.*, vol. 6, pp. 1–7, Apr. 2016, doi: 10.1038/srep24385.

[24] F. Yesilkoy et al., "Phase-sensitive plasmonic biosensor using a portable and large field-of-view interferometric microarray imager," *Light Sci. Appl.*, vol. 7, no. 2, p. 17152, 2018, doi: 10.1038/lsa.2017.152.

[25] J. K. Levy, P. C. Crawford, W. R. Collante, and M. G. Papich, "Use of adult cat serum to correct failure of passive transfer in kittens," *J. Amer. Vet. Med. Assoc.*, vol. 219, no. 10, pp. 1401–1405, Nov. 2001, doi: 10.2460/javma.2001.219.1401.

[26] R. Harley, T. J. Gruffydd-Jones, and M. J. Day, "Determination of salivary and serum immunoglobulin concentrations in the cat," *Vet. Immunol. Immunopathol.*, vol. 65, nos. 2–4, pp. 99–112, 1998, doi: 10.1016/S0165-2427(98)00146-9.

[27] C. Kluge, "Nanostructures for emission control in organic light-emitting layers," Ph.D. dissertation, Dept. Elect. Inf. Eng., Chair Integr. Syst. Photon., Kiel Univ., Kiel, Germany, 2014.

[28] T. Frank, O. Buchnev, T. Cookson, M. Kaczmarek, P. Lagoudakis, and V. A. Fedotov, "Discriminating between coherent and incoherent light with planar metamaterials," *Nano Lett.*, vol. 19, no. 10, pp. 6869–6875, Oct. 2019, doi: 10.1021/acs.nanolett.9b02094.

[29] X. Chong et al., "Detect the hybridization of single-stranded DNA by parallel scan spectral surface plasmon resonance imaging," *Plasmonics*, vol. 8, no. 2, pp. 1185–1191, 2013, doi: 10.1007/s11468-013-9530-1.

[30] M. L. Gorodetsky, A. A. Savchenkov, and V. S. Ilchenko, "Ultimate Q of optical microsphere resonators," *Opt. Lett.*, vol. 21, no. 7, pp. 453–455, Apr. 1996.

[31] D. Conteduca, G. S. Arruda, I. Barth, Y. Wang, T. F. Krauss, and E. R. Martins, "Beyond Q: The importance of the resonance amplitude for photonic sensors," *ACS Photon.*, vol. 9, no. 5, pp. 1757–1763, May 2022, doi: 10.1021/acsphotonics.2c00188.

[32] R. R. Boye and R. K. Kostuk, "Investigation of the effect of finite grating size on the performance of guided-mode resonance filters," *Appl. Opt.*, vol. 39, no. 21, pp. 3649–3653, 2000, doi: 10.1364/ao.39.003649.

[33] G. A. Turnbull, P. Andrew, M. J. Jory, W. L. Barnes, and I. D. W. Samuel, "Relationship between photonic band structure and emission characteristics of a polymer distributed feedback laser," *Phys. Rev. B, Condens. Matter*, vol. 64, no. 12, pp. 1–6, Sep. 2001, doi: 10.1103/PhysRevB.64.125122.

[34] K. Li et al., "Extended Kalman filtering projection method to reduce the 3σ noise value of optical biosensors," *ACS Sensors*, vol. 5, no. 11, pp. 3474–3482, 2020, doi: 10.1021/acssensors.0c01484.

[35] A. F. Coskun, A. E. Cetin, B. C. Galarreta, D. A. Alvarez, H. Altug, and A. Ozcan, "Lensfree optofluidic plasmonic sensor for real-time and label-free monitoring of molecular binding events over a wide field-of-view," *Sci. Rep.*, vol. 4, no. 1, pp. 1–7, Oct. 2014, doi: 10.1038/srep06789.

[36] Y. Tie, C. Calonder, and P. R. Van Tassel, "Protein adsorption: Kinetics and history dependence," *J. Colloid Interface Sci.*, vol. 268, no. 1, pp. 1–11, 2003, doi: 10.1016/S0021-9797(03)00516-2.

[37] T. Urbanowska, S. Mangialaio, C. Hartmann, and F. Legay, "Development of protein microarray technology to monitor biomarkers of rheumatoid arthritis disease," *Cell Biol. Toxicol.*, vol. 19, no. 3, pp. 189–202, 2003, doi: 10.1023/A:1024729526867.

[38] K. A. Brokstad, R. J. Cox, J. Olofsson, R. Jonsson, and L. R. Haaheim, "Parenteral influenza vaccination induces a rapid systemic and local immune response," *J. Infectious Diseases*, vol. 171, no. 1, pp. 198–203, Jan. 1995, doi: 10.1093/infdis/171.1.198.

[39] G. W. Schael, "Determination of polyolefin film properties from refractive index measurements. II. Birefringence," *J. Appl. Polym. Sci.*, vol. 12, no. 4, pp. 903–914, Apr. 1968, doi: 10.1002/app.1968.070120424.

[40] P. R. Pinnock and I. M. Ward, "Mechanical and optical anisotropy in polypropylene fibres," *Brit. J. Appl. Phys.*, vol. 17, no. 5, pp. 575–586, May 1966, doi: 10.1088/0508-3443/17/5/301.

Fabio A. Kraft was born in Germany, in 1989. He received the master's degree in microtechnology and nanotechnology from the University of Technology Ilmenau, Ilmenau, Germany, in 2015.

After that, he worked for the optic metrology manufacturer trioptics before starting his Ph.D. degree at the Chair for Integrated Systems and Photonics, Kiel University, in 2020. His research interests include biosensing with photonic crystal slabs for point-of-care devices and wearable applications.

Jan Schardt was born in Germany, in 1992. He received the master's degree in electrical engineering and information technology from Kiel University, Kiel, Germany, in 2018, where he is currently pursuing the Ph.D. degree with the Chair for Integrated Systems and Photonics, Institute of Electrical Engineering.

His research interests include semitransparent and flexible organic optoelectronics and the integration of nanostructures in organic photodetectors.

Deborah Kitzler was born in Atlanta, GA, USA, in 2001. She is currently pursuing the bachelor's degree in biomedical engineering with the Georgia Institute of Technology, Atlanta, GA, USA.

She has previously worked in labs studying muscle protein assembly, maintenance and regulation in biological systems, and drug development and resistance in viral systems, specifically human immunodeficiency virus (HIV). Her interests for future research include drug delivery systems, virology, and diagnostic techniques using biosensors.

Andreas Latz was born is Neukirchen beim Heiligen Blut, Germany, in 1974. He received the Diploma and Ph.D. degrees in biology from the Julius Maximilian University Würzburg, Würzburg, Germany, in 2002 and 2007, respectively.

He worked as a Post-Doctor and the Group Leader at the Eberhard Karls University Tübingen, Tübingen, Germany. Since 2010, he has been working with NovaTec Immundiagnostica GmbH, Dietzenbach, Germany, where he is also the Head of the Veterinary Diagnostic Department.

Martina Gerken (Senior Member, IEEE) received the Dipl.-Ing. degree from the University of Karlsruhe, Karlsruhe, Germany, in 1998, and the Ph.D. degree from Stanford University, Stanford, CA, USA, in 2003, all in electrical engineering.

From 2003 to 2008, she was an Assistant Professor at the University of Karlsruhe. She was appointed as a Full Professor of electrical engineering and the Head of the Chair for Integrated Systems and Photonics, Kiel University, Kiel, Germany, in 2008. She is currently a Full Professor with Kiel University.